Investigating beach erosion related with tsunami sediment transport at Phra Thong Island, Thailand caused by the 2004 Indian Ocean tsunami

Ryota Masaya [1], Anawat Suppasri [2], Kei Yamashita [2], Fumihiko Imamura [2], Chris Gouramanis [3] and Natt Leelawat [4, 5]

[1]Graduate School of Engineering, Tohoku University, Aoba-yama 6-6-06, Aoba-ku, Sendai 980-0845, Japan
[2]International Research Institute of Disaster Science, Tohoku University, 468-1 Aoba, Aramaki-Aza, Aoba-ku, Sendai 980-0845, Japan
[3]Department of Geography, National University of Singapore, 1 Arts Link, Singapore 117570, Singapore
[4]Department of Industrial Engineering, Faculty of Engineering, Chulalongkorn University, Phayathai Road, Pathumwan, Bangkok 10330, Thailand
[5]Disaster and Risk Management Information Systems Research Group, Chulalongkorn University, Phayathai Road, Pathumwan, Bangkok 10330, Thailand
*Corresponding author.
E-mail address: ryota.masaya.r6@dc.tohoku.ac.jp (Ryota Masaya)

Abstract

The 2004 Indian Ocean Tsunami and the 2011 Great East Japan earthquake and tsunami caused large-scale topographic changes in coastal areas. Whereas much research has focused on coastlines that have or had large human populations, little focus has been paid on coastlines that have little or no infrastructure. The importance of examining erosional and depositional mechanisms of tsunami events lies in the rapid reorganisation that coastlines must undertake immediately after an event. Through understanding the precursor conditions to this reorganisation is paramount to the reconstruction of the coastal environment. This study examines the location of sediment erosion and deposition during the 2004 Indian Ocean Tsunami event on the relatively pristine Phra Thong Island, Thailand. Coupled with satellite imagery, we use numerical simulations and sediment transportation models to determine the locations of significant erosion and the areas where much of that sediment was redeposited during the tsunami inundation and backwash processes. Our modelling approach suggests that beaches located in two regions on Phra Thong Island were significantly eroded by the 2004 tsunami, predominantly during the backwash phase of the first and largest wave to strike the island. Although 2004 tsunami sediment deposits are found on the island, we demonstrate that most of the sediment was deposited in the shallow coastal area, facilitating quick recovery of the beach when normal coastal processes resume.

1. Introduction

The 2004 Indian Ocean Tsunami and the 2011 Great East Japan earthquake and tsunami caused large-scale geomorphologic changes in coastal areas during the erosional phases of inflow and outflow (Pari et al., 2008; Goto et al., 2011a; Tanaka et al., 2011; Haraguchi et al., 2012; Hirao et al., 2012; Udo et al., 2013; Imai et al., 2015). In each tsunami event, the erosional phases translocated sediments onshore and offshore and primed the coastal zone for rapid (months to decades) recovery (Choowong et al., 2009; Ali et al., 2015; Udo et al., 2016; Mieda et al., 2017; Koiwa et al., 2018). However, little information exists to identify real-time sediment dynamics during the erosional and depositional phases of tsunami events. In particular, erosive phases mobilise sediments into the onshore (e.g. Jankaew et al. 2008; Gouramanis et al. 2017) and offshore environments (e.g. Feldens et al 2009). Following the tsunami event, both offshore environment and coastal environments are primed for natural processes to resume and redistribute sediments onshore to restore the coastal environment to similar pre-tsunami configurations.

However, in many regions, such as the area affected by the 2011 tsunami, extensive engineering interventions (e.g. levee construction and land level raising) are affecting the natural recovery processes of the coastal zone. In Japan, many locations have not undergone or been allowed to recover naturally (Udo et al., 2016; Koiwa et al., 2018), as engineering interventions have taken precedence over natural recovery processes.

Along highly developed and populated coasts that have been affected by tsunami, e.g. Japan, plans for coastal reconstruction and defenses are typically formulated shortly after time after a tsunami, preventing natural recovery processes (Suppasri et al., 2016). These political and engineering interventions make it difficult to observe or predict the natural recovery processes of coastal areas.

Immediately following a tsunami event, the sediment dynamics of the coastal zone are largely modified with sediment having been eroded and deposited elsewhere, either onshore (e.g. Jankaew et al. 2008; Gouramanis et al. 2017) or offshore (e.g. Feldens et al. 2009). Before an understanding of the recovery processes of a tsunami-affected coastal zone can be achieved, a thorough understanding of the sediment budget must be determined. The relocation of sediments during the main tsunami erosion and deposition phases establishes the pre-recovery or baseline conditions upon which natural processes can act to facilitate the recovery of the coastal zone. To determine the locations of sediment deposition during a tsunami event, the sediment transport dynamics during the tsunami must be defined.

Unfortunately, real-time data from observations has not been possible to establish quantitative estimates of sediment erosion and deposition during a tsunami event. Prior studies have mainly estimated sediment transport dynamics, such as erosion and sediment deposition through remote sensing (e.g. Fagherazzi & Du 2008, Choowong et al., 2009; Liew et al., 2010), and sedimentological and stratigraphic analysis (e.g. Paris et al. 2007; Hawkes et al. 2007; Switzer et al. 2012). However, the information obtained regarding the final results of the sediment transport process is limited. It is difficult to obtain information on where sediment has eroded and deposited (e.g. Pham et al 2018), and whether topographic changes caused by the local sediment runoff or deposition are the results of action from inflow or backwash (e.g. Choowong et al., 2009; Paris et al 2007; Switzer et al. 2012). This information determines the sediment budget in the system before and after the tsunami and is therefore important for considering geomorphic recovery.

Numerical simulations using wave dynamics of an area can reproduce spatial-temporal variations of the sediment mobility and deposition and can effectively model the sediment transport process using the wave and sediment characteristics of the natural system. In recent years, the numerical modeling of tsunami sediment transport has been developed, improved and applied in the field (Takahashi et al., 1999; Gelfenbaun et al., 2007; Takahashi et al., 2008; Apotsos et al., 2011a; Apotsos et al., 2011b; Apotsos et al., 2011c; Takahashi et al., 2011; Gusman et al., 2012; Li et al., 2012; Takahashi et al., 2012; Li et al., 2014; Morishita & Takahashi, 2014; Yamashita et al., 2015; Yamashita et al., 2016; Arimitsu et al., 2017; Yamashita et al., 2017; Yamashita et al., 2018), and reproducibility has been confirmed by comparison between the calculated and measured values (Yamashita et al., 2015; Yamashita et al., 2016; Arimitsu et al., 2017; Yamashita et al., 2017; Yamashita et al., 2018).

An important consideration in the sediment dynamics during catastrophic marine events (e.g. typhoon and tsunami) is the degree of development and human modification of the coastal zone prior to the event. Artificial structures, such as sea walls, roads and buildings interfere with washover processes, and these areas are often targeted from reconstruction and rehabilitation through rapid engineering reconstruction. Little is known about the recovery processes in sparsely developed and unpopulated areas. As such, largely anthropogenically undisturbed Phra Thong Island, western Thailand, is an ideal location to model the sediment dynamics, coastal erosion and deposition following a major tsunami event.

Examining the sediment transport processes on Phra Thong Island is expected to elucidate phenomena, improve numerical calculation models for the future and is applicable to other areas. Furthermore, at least three palaeotsunami deposits were identified in areas impacted by the 2004 IOT on Phra Thong Island (Jankaew et al., 2008; Sawai et al., 2009; Fujino et al., 2009; Fujino et al., 2010; Prendergast et al. 2012; Brill et al., 2012a, b; Gouramanis et al., 2017; Pham et al., 2018). Thus, clarifying the sediment transport conditions of the 2004 tsunami will be important for future estimations of history, scope and cause of older tsunamis on Phra Thong Island and elsewhere in the coastal areas of the Indian Ocean.

This study investigates the conditions of sediment transport and establishes the baseline sediment conditions that led to the recovery of the Phra Thong Island coastline after the 2004 IOT. We used tsunami sediment transport calculations to spatio-temporally reproduce the sediment transport processes occurring during the tsunami and identify zones of sediment deposition in the offshore and onshore areas and validate these modelling results with published observational data of the 2004 IOT deposits on the island. Due to the largely natural environment, Phra Thong Island is a rare case that is useful for verifying tsunami sediment transport models where few artificial features can generate model uncertainties.

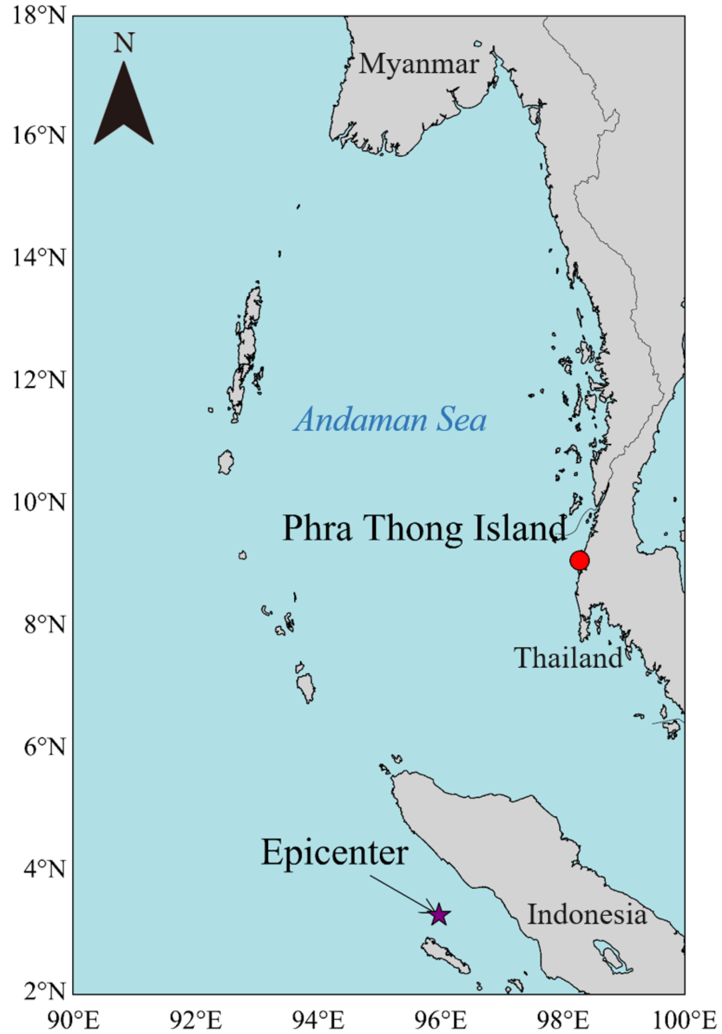

Figure 1 Location of Phra Thong Island

2. Setting and method

2.1. *Phra Thong Island, Thailand*

During the 2004 IOT, a wave of approximately 7 m inundated the northern portion of Phra Thong Island and measurements up to 20 m were recorded from the southernmost tip of the island (Jankaew et al. 2008; Fig.1). Over 70 people were lost and a village of 100 households disappeared. Geomorphologically, the western coast of the island has a beach ridge sequence trending parallel to the coast, which formed during the sea level regression following mid-Holocene sea level highstand at *ca.* 6,000 years ago (Brill et al. 2015). The eastern shore of the island is extensively covered by mangroves along the shores of tidal channels. The island has a tropical climate. Additionally, palaeotsunami deposits are preserved in swales in the beach ridge system along the western coast of Thailand (e.g. Jankaew et al. 2008; Gouramanis et al. 2017). Furthermore, although local beaches were lost in the 2004 tsunami, satellite photography showed recovery within 18 months (e.g. Choowong et al. 2009).

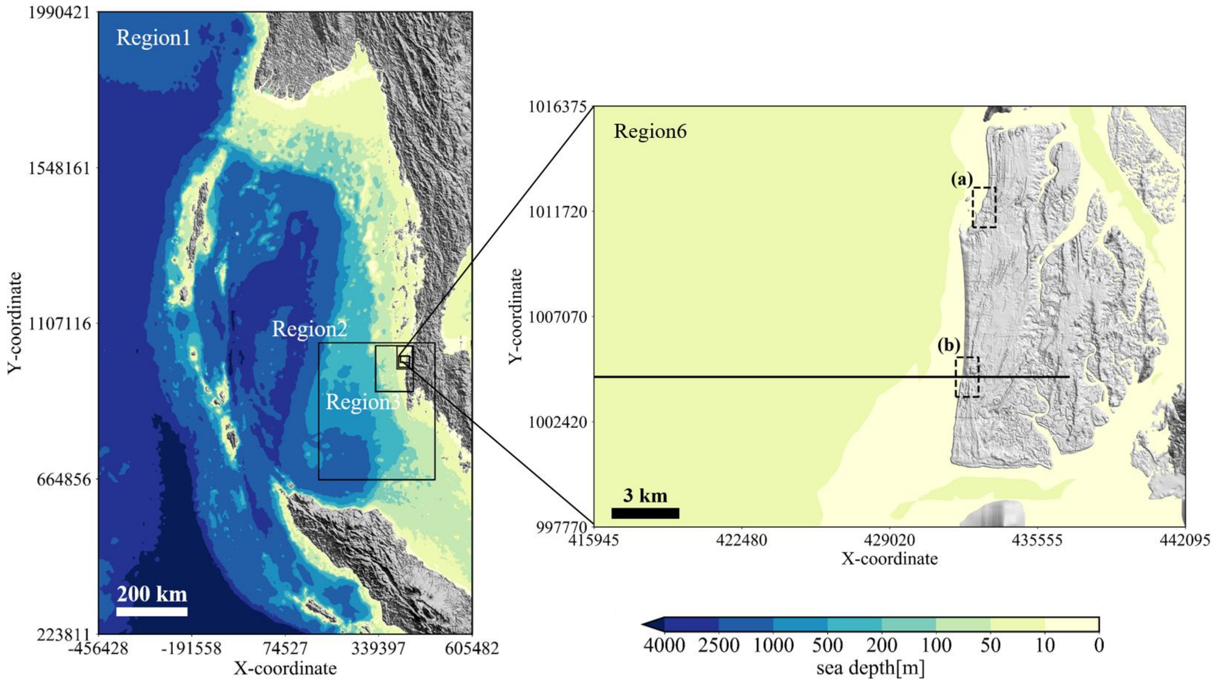

Figure 2 Terrain data (The black frame shows Region 1 to Region 6, and the black line in Region 6 shows the cross-section where calculation was performed. Dashed squares are the beach where erosion was confirmed from satellite image.)

2.2. *Topography and bathymetry data*

The topography and bathymetry data used for the tsunami sediment transport calculations were created based on various water depths and elevations. Figure 2 shows the terrain data that were created. Topographic data were downscaled from Region 1, which includes the Andaman Sea, to Region 6, which includes all of Phra Thong Island. The grid spacing decreases from 1,215 m^2 for Region 1 to 5 m^2 for Region 6. In the tsunami sediment transport calculations, UTM zone 47N was used to geospatially constrain the horizontal modelling coordinates of the target area Phra Thong Island. Region 1 is the projection of depth data of the 30-second grid provided by GEBCO (2014) on the Cartesian coordinate system UTM 47N. Regions 2–4 use a digital marine chart with 300 m resolution based on a survey by the Thai Navy. Regions 5 and 6 use an original 5 m (terrain data) and 15 m (sea depth data) grid spacing to create mean terrain and water depth data based on analysis of satellite image by EOMAP and elevation data provided by the Land Development Department of Thailand. The terrain data of Region 4, created from the digital marine chart of 300 m resolution, showed discontinuity at the boundary with Region 5, which had a higher resolution. The discontinuity was therefore removed to the extent possible by interpolation with an inverse distance weighting method using all terrain data.

2.3. *Tsunami source model*

The fault model proposed by Suppasri et al. (2011) was used as the tsunami source of the 2004 Indian

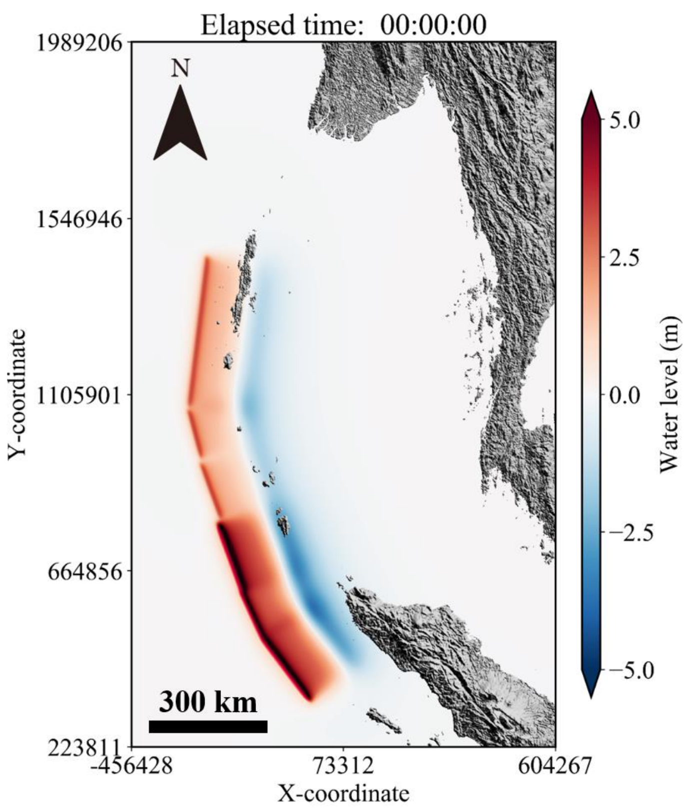

Figure 3 Initial water level after earthquake occurrence

Table 1 Earthquake fault parameters for calculating initial water level (Suppasri et al., 2011)

Segment No.	1	2	3	4	5	6
Latitude(°N)	3.03	4.48	5.51	7.14	8.47	9.63
Longitude(°E)	94.40	93.32	92.87	92.34	91.88	91.57
Strike(deg)	323	335	340	340	345	7
Dip(deg)	15	15	15	15	15	15
Slip(deg)	90	90	90	90	90	90
Length(km)	200	125	180	145	125	380
Width(km)	150	150	150	150	150	150
Dislocation(m)	14	12.6	15.1	7	7	7
Depth(km)	10	10	10	10	10	10

Ocean Tsunami. Suppasri et al.'s (2011) source model was focused on the coast of Thailand and accurately reproduced the inundation area and surveyed trace height of the 2004 IOT. The fault model is divided into six small faults from satellite image analysis and survey results, and it is assumed that each small fault slides simultaneously and instantaneously. For the tsunami source, the vertical tectonic displacement in each fault was calculated according to Okada (1985). Table 1 shows the fault parameters of each fault and Figure 3 shows the initial water level.

2.4. *Tsunami sediment transport calculation*

2.4.1. *Tsunami propagation and run-up model*

Tohoku University's Numerical Analysis Model for Investigation of Near-field tsunamis, No. 2 (TUNAMI-N2) is based on the nonlinear long wave theory and was used as the tsunami propagation and run-up model.

$$\frac{\partial \eta}{\partial t} + \frac{\partial M}{\partial x} + \frac{\partial N}{\partial y} = 0 \tag{1}$$

$$\frac{\partial M}{\partial t} + \frac{\partial}{\partial x}\left(\frac{M^2}{D}\right) + \frac{\partial}{\partial y}\left(\frac{MN}{D}\right) + gD\frac{\delta \eta}{\delta x} + \frac{gn^2}{D^{\frac{7}{3}}} M\sqrt{M^2 + N^2} = 0 \tag{2}$$

$$\frac{\partial N}{\partial t} + \frac{\partial}{\partial x}\left(\frac{MN}{D}\right) + \frac{\partial}{\partial y}\left(\frac{N^2}{D}\right) + gD\frac{\delta \eta}{\delta y} + \frac{gn^2}{D^{\frac{7}{3}}} N\sqrt{M^2 + N^2} = 0 \tag{3}$$

Here, η is the change in water level from the still-water surface, D is the total water depth from the bottom to the water surface, and g is the acceleration of gravity. The bottom friction is expressed according to the Manning formula, where n is Manning's roughness coefficient. M and N are the total flow fluxes in the x and y directions, respectively, and are given by integrating the horizontal flow velocity u, v from the water bottom h to the water surface η. It is assumed that the horizontal flow velocity is uniformly distributed in the vertical direction.

The nonlinear long wave theory consists of a continuous equation that is derived from (1) the principle of conservation of mass (continuity equation) and (2) the conservation of momentum (equation of motion). These two equations are obtained by vertically integration from the seabed to the water surface.

When the water depth is about 50 m or less, the effects of the 2nd, 3rd and 5th terms of the advection and seabed friction terms (Equations 2 and 3) are reduced, therefore wave theory that omit these terms is often used at depths shallower than 50 m. Meanwhile, the Message Passing Interface (MPI) parallel was implemented in the model for highly efficient calculations. Both the advection term and the bottom friction term were therefore considered in the calculations without reducing accuracy in deeper waters.

The reproducibility of the calculated results is based on the tsunami height data (IUGG; available at http://www/nda.ac.jp/fu-jima/TMD/index.html) for the 2004 IOT and is discussed using the geometric mean K and geometric standard deviation κ proposed by Aida (1978).

$$\log K = \frac{1}{n}\sum_{i=1}^{n} \log K_i \tag{4}$$

$$\log\kappa = \sqrt{\frac{1}{n}\left\{\sum_{i=1}^{n}(\log K_i)^2 - n(\log K)^2\right\}} \tag{5}$$

Here, n is the number of points, R_i is the tsunami height at the i^{th} point, H_i is the calculated value at the ith point, and $K_i = R_i/H_i$.

2.4.2. *Sediment transport model*

For the tsunami movable bed model, we used the numerical sediment transport model (STM) proposed by Takahashi et al. (2000), which solves the time evolution of sediment transport considering the exchange sediment volume of the bed and suspended load layers according to the flow conditions of the nonlinear long wave theory-based TUNAMI-N2 model. For each time step, the STM receives the total flow fluxes from TUNAMI-N2 and calculates the change of seafloor and land surface and feeds this to the next time step of the TUNAMI-N2 model.

This model divides tsunami sediment transport into a bed load layer, where sediment grains pull, and a suspended load layer, where sediment grains float. The governing equations consist of continuous equations for the bed load layer and the suspended load layer:

$$\frac{\partial Z_B}{\partial t} + \frac{1}{1-\lambda}\left(\frac{\partial q_{B_x}}{\partial x} + \frac{\partial q_{B_y}}{\partial y} + \omega_{ex}\right) = 0 \tag{6}$$

$$\frac{\partial \bar{C}_s M}{\partial x} + \frac{\partial \bar{C}_s N}{\partial y} - \omega_{ex} + \frac{\partial \bar{C}_s h_S}{\partial t} = 0 \tag{7}$$

Equation (6) is a continuous equation for within the bed load layer. The first term is the exchange sediment volume with the bottom, the second term is the balance of sediment flow volume moving in a tractive form in the flow direction, and the third term defines the balance of suspension flux, caused by diffusion, and sedimentation flux, caused by gravity, as the exchange sediment volume between the bed load layer and the suspended load layer. ω_{ex} is expressed by the following equation.

$$\omega_{ex} = \varepsilon_z \frac{\partial C}{\partial z} - \omega_0 C \tag{8}$$

Here, ρ_s is the sediment grain density, λ is the sediment grain porosity, Z_B is the bottom height from the reference plane, q_B is the amount of bed load sediment, ε_z is the diffusion coefficient in the vertical direction, C is the concentration in the vicinity of the boundary between the bed load layer and the suspended sediment layer, ω_0 is the sedimentation velocity of the sediment grains, C_B is the average bed load sediment concentration, h_B is the bed load layer thickness, C_S is the average suspended load layer concentration, h_s is the suspended load layer thickness, and M is the bed load flux. w_0 is the sedimentation velocity of the sediment grains.

Equation (7) is a continuous equation for within the suspended load layer. The first and second terms are bed load sediment moving in a suspended state in the flow direction, the third term is the exchange sediment volume between the bed load layer and the suspended load layer, and the fourth term is the increase or decrease of the sediment flow in the suspended load layer.

In Equations (6) and (7), the equation defining the bed load sediment volume q_B and the equation defining the exchange sediment volume w_{ex} of the bed load layer and suspended load layer are necessary, but according to Takahashi et al. (1999), they are obtained by the following:

$$q_B = \alpha\sqrt{sgd^3}(\tau_* - \tau_c)^{\frac{3}{2}} \tag{9}$$

$$\omega_{ex} = \beta\sqrt{sgd}(\tau_* - \tau_c)^2 - \omega_0\bar{C}_s \tag{10}$$

$$\tau_* = \frac{u_*^2}{sgd} \tag{11}$$

Here, α is the coefficient of the bed load sediment volume equation, β is the coefficient of the suspension volume equation, s is specific gravity in water, g is the acceleration of gravity, d is grain diameter, τ_* is the Shields number, τ_c is the limit Shields number, u_* is the friction velocity obtained from the Manning formula. The grain-size dependent parameter for bed load (α) and exchange rate (β) in Equation (9) and (10) are derived from Equations (12) and (13) based on the hydraulic experiments by Takahashi et al. (2011):

$$\alpha = 9.8044e^{-3.366d} \tag{12}$$

$$\beta = 0.0002e^{-6.5362d} \tag{13}$$

However, the functions should not be applied when d is outside the 0.166 mm to 0.394 mm range as he validity of extrapolated d values may produce erroneous results.

In Equation (6) and Equation (7), the bottom height (Z_B) is determined from the reference plane, and the average suspended sediment concentration (C_S) are the initial values before the tsunami and the flow flux (M). Because suspended sediment thickness (h_S) is given by the equation of motion of a fluid and the continuous equation, sea level fluctuation can be determined over time. Further, the MPI parallel was implemented to enable relatively efficient wide area calculations (e.g. Yamashita et al. 2016).

2.5. *Calculation conditions*

The conditions for the numerical simulations used the terrain data (Figure 2) and tsunami source (Figure 3). The simulations were performed using a 3:1 nested grid that increased the resolution a 1215 m^2 grid to a 5 m^2 grid. Additionally, the target region of the sediment transport calculation was limited to Region 6, with a grid spacing of 5 m^2.

The simulations were calculated over a 0.05 second increment with a 6 hour period in which the test case with a 12 hour period showed the suspended sediment concentration in the vicinity of the shoreline decreased and stabilized.

For the bottom conditions, the Manning's roughness coefficient was fixed at n = 0.030 s/$m^{1/3}$, and the entire area of Region 6 was considered the movable bed. In general, when simulating tsunami sediment transport, it is necessary to determine the roughness coefficient according to land use. However, since there is no land use map before the tsunami on Phra Thong Island, a fixed value was used, similar to previous studies (Yamashita et al., 2017; Yamashita et al., 2018). Sugawara et al. (2014b) showed that the variation in Manning's roughness coefficient for the sand beds may affect the general distribution pattern of sediment deposits and erosions across the artificial topographic features. Therefore, we do not analyze the sensitivity of Manning's roughness because Phra Thong Island has little artificial features.

The grain size was based on one sediment data set (Gouramanis et al., 2017) from the locally eroded region, and was considered as a representative value for all of the tsunami sediment grain sizes. A uniform grain size of D_{50} = 0.127 mm was used. The Critical Shields number τ_c in Equations (9) and (10) was obtained using Equations (12) and (13) according to Iwagaki et al. (1954):

$$\tau_c = u_c^2 \rho \tag{12}$$

$$u_c^2 = 8.41 d^{\frac{11}{32}} \tag{13}$$

Here, u_c is the critical friction and ρ is the density of water. Table 2 shows each parameter used for the sediment transport calculations in this study.

The numerical model used in this paper can only consider a single grain size, so the model cannot resolve the grading of the sand layer. Additionally, initial bed grain size can have a large effect on erosion and deposition (e.g. Apotsos et al., 2011; Sugawara et al., 2014; Jaffe et al., 2016). Furthermore, the sediment data we used to set the grain size is only one point on the north side, so it cannot be said that it is sufficient data to set the representative grain size. Therefore, it is necessary to perform sensitivity analysis on grain size. Pham et al. (2018) investigated the surface grain size of the offshore (water depth > 15 m), nearshore (water depth < 15 m), and onshore on Phra Thong Island, which is considered to be the source of tsunami deposits. As the result, the mean grain size was 0.314 mm in the offshore, 0.129 mm in the nearshore, and 0.285 mm in the onshore. Based on these information, we

Table 2 Set parameters for sediment transport calculations

Parameter	Value
Coefficient of bed load sediment volume equation α	6.40
Coefficient of suspension sediment volume equation β	8.70×10^{-5}
Critical friction u_c	0.0137 m/s
Bottom slope correction factor ε_z	2.5
Sedimentation velocity of sediment grains w_0	0.0971 m/s
Maximum suspended sediment concentration C_{max}	37.7%
Specific gravity of sediment grains in water s	1.65
Void ratio λ	0.4

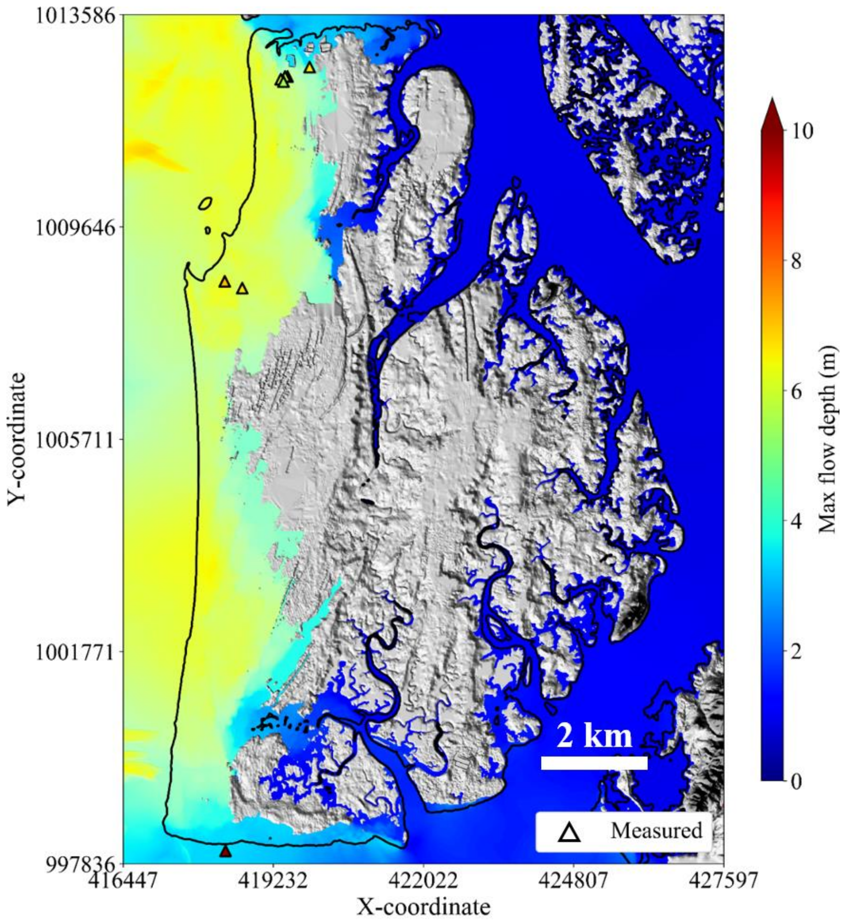

Figure 4 Comparison of calculated and measured maximum flow depth

tested sensitivity analysis for two grain sizes at 0.285 mm from offshore and 0.314 mm from onshore.

3. Result

3.1. *Verification of reproducibility*

3.1.1. *Tsunami height*

Figure 4 shows the results of the calculation of the maximum tsunami height and the seven measured heights on Phra Thong Island.

From Equations (12) and (13), $K = 0.96$ and $\kappa = 1.1$ are obtained. Additionally, the source model used in this calculation gives $K = 0.84$ and $\kappa = 1.3$ for reproducibility of tsunami ~~trace~~ height in the wide area along the coast of Thailand (Suppasri et al., 2011). The Japan Society of Civil Engineers (2012) consider $0.95 < K < 1.05$ and $\kappa < 1.45$ as guides for evaluating reproducibility of tsunami numerical calculations. Therefore, it can be said that this calculation has good tsunami reproducibility.

3.1.2. *Change of shoreline*

Our sediment transport models identify the locations of significant sediment erosion, which are confirmed from post-tsunami satellite images. Figure 5 shows the pre-2004 IOT topographical and

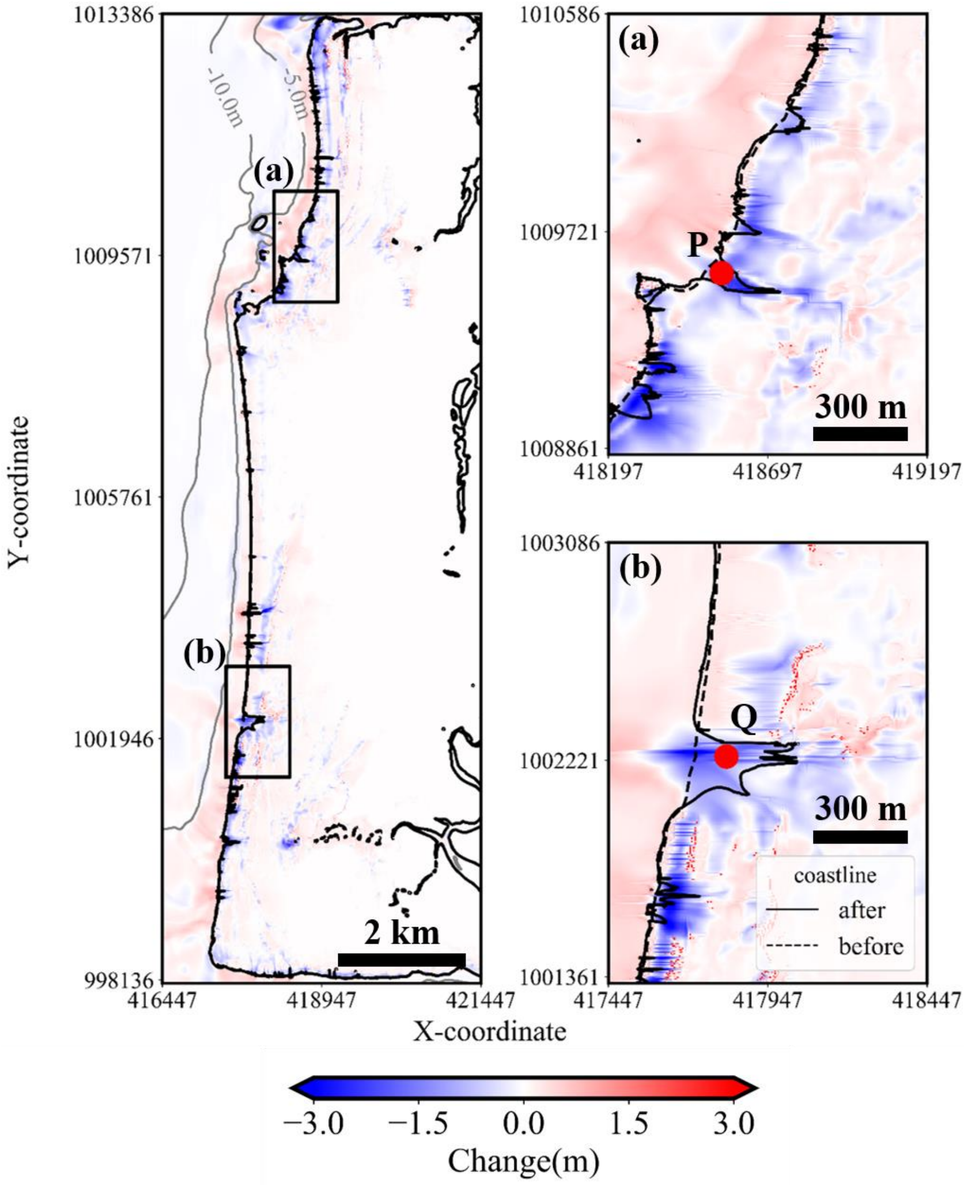

Figure 5 Topographic change and shoreline position caused by the tsunami(solid & dashed lines show that the coastline after and before the tsunami in the simulation, P and Q are the points confirmed

local beach erosion in region (a) and (b), blue and red mapping show erosion and deposition after the tsunami in the simulation)

geomorphological features (dashed line) and the modelled changes caused by the tsunami (solid line). Erosion typically occurs locally where small tidal channels breach the youngest beach ridge system (Figure 5a and 5b). Comparison with the satellite image shows that the position of erosion in both regions is consistent (Figure 6). Although the actual amount of erosion is unknown, this indicates that the planar spread of the eroded part can be relatively well reproduced relatively by the calculation. Region (a) was further investigated in detailed as the area corresponds to the point where sediment outflow was confirmed by Jankaew et al. (2008) in the following section.

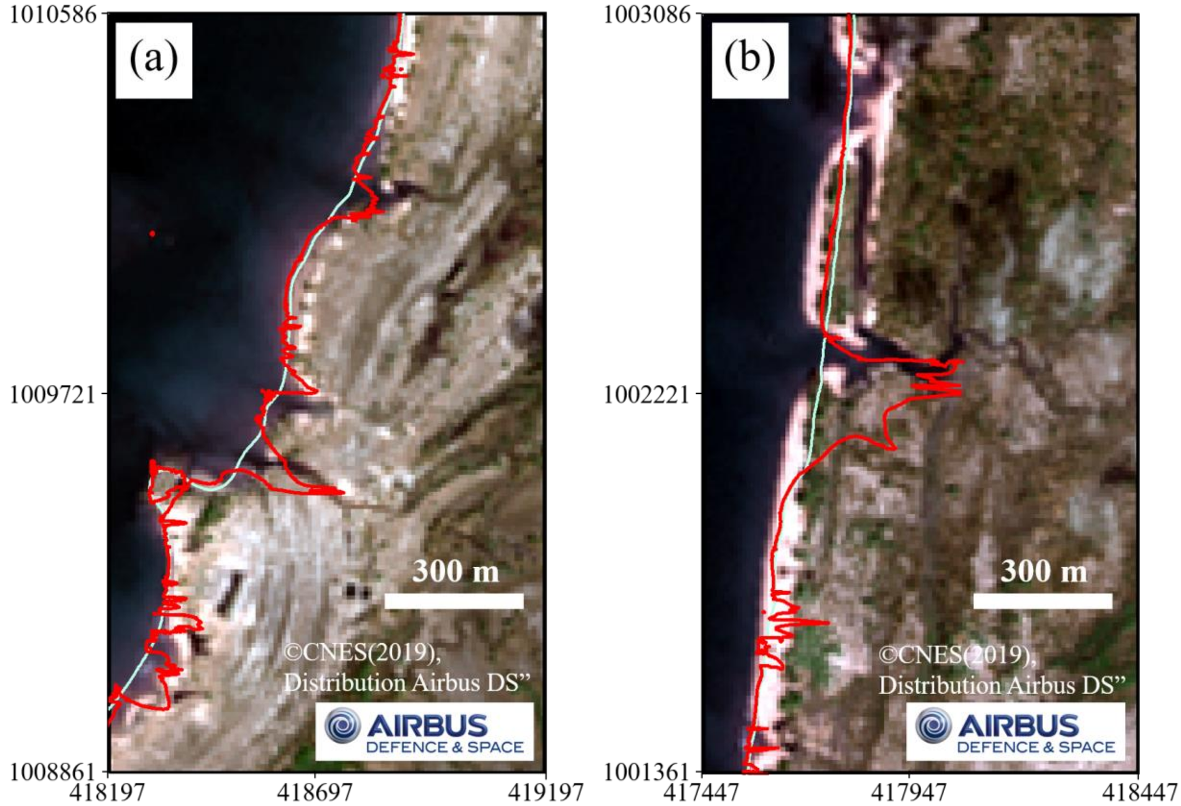

Figure 6 Comparison of observed shoreline position from Figure 5 region (a) and (b) derived from satellite image (30 Jan, 2005), which is overlain by the modelled extent of erosion showing that the modelled results closely match the observed changes. The red line is the calculated shoreline after the tsunami, and the blue line is the shoreline before the tsunami (© CNES, 2019, Distribution Airbus DS")

3.1.3. *2004 IOT onshore sediment deposition*

In addition to the erosional features, the model simulated the deposition of 2004 IOT sediments across the island. The thickness of these simulated deposits are compared with 148 measured 2004 IOT deposit thicknesses (Jankaew et al., 2008; Gouramanis et al., 2017).

The line of "volume" show the cumulative deposition expressed at each point by the sediment thickness multiplied by the area of the computational grid. In general, the tsunami deposits are greatly affected by local micro-topography(Sugawara et al., 2014; Jaffe et al., 2016), and it is difficult to fit the modelled layer thickness with the observed layer thickness using DEM averaged in a computational grid. Therefore, we introduced the concept of cumulative sedimentation, and evaluated the scale of the amount of sediment movement generated. Although the modelled layer thickness typically overestimates the observed layer thickness by +7%, such low variation suggests a relatively successful reproduction of the observed dataset (Figure 7). The modelled overestimation is likely due to the assumption that the entire exposed land area would act as a movable bed. In reality, this is an oversimplification of the true ground surface, which contains vegetation that binds and traps the soil

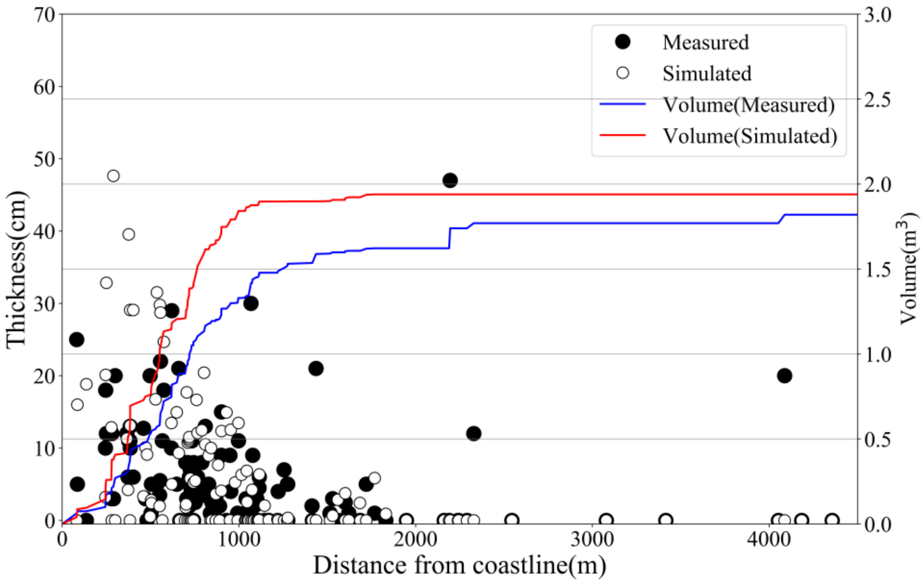

Figure 7 Comparison of field measured and simulated tsunami deposit thickness using a representative grain size of d = 0.127 mm. Black point shows the measured thickness by Jankaew et al.(2008) and Gouramanis et al.(2017), white point shows the simulated thickness. Blue and red line show the cumulative curves of measured data and simulated data.

Table 3 volume of erosion and deposition in regions (a) and (b) for each grain size (Percentage shows the ratio to reference)

	d (mm)	Erosion(m^3)		Deposition(m^3)	
		Region (a)	Region (b)	Region (a)	Region (b)
Reference	0.127	352,333	314,189	259,379	254,417
Onshore	0.285	143,793(41%)	155,225(49%)	161,810(62%)	149,470(59%)
Offshore	0.314	117,491(33%)	128,289(41%)	137,749(53%)	128,801(51%)

and wet regions (i.e. in swales) that would have higher degrees of sediment cohesion, reducing the area that would be eroded. In addition, the model also reproduces the inland thinning of the 2004 IOT deposit (Figure 7).

3.1.4. *Sensitivity analysis for grain size and roughness*

Figure 8, 9 and 10 shows the topographical changes andthickness of sediment layer in this calculation for each grain size, and Table 3 shows the volume of erosion and deposition in regions (a) and (b). These evidences show that smaller the particle size is, the greater the topographic change. This can be understood by the smaller the particle size, the larger the Shields number in Eq. (11), which indicates the ease of sediment transport, and the greater the amount of bed load in Eq. (9). However, Figure 8 suggested that the qualitative characteristics of sediment transport are same in the three cases, due to the local erosion position of the beach in region (a) and (b) did not change for any particle size.

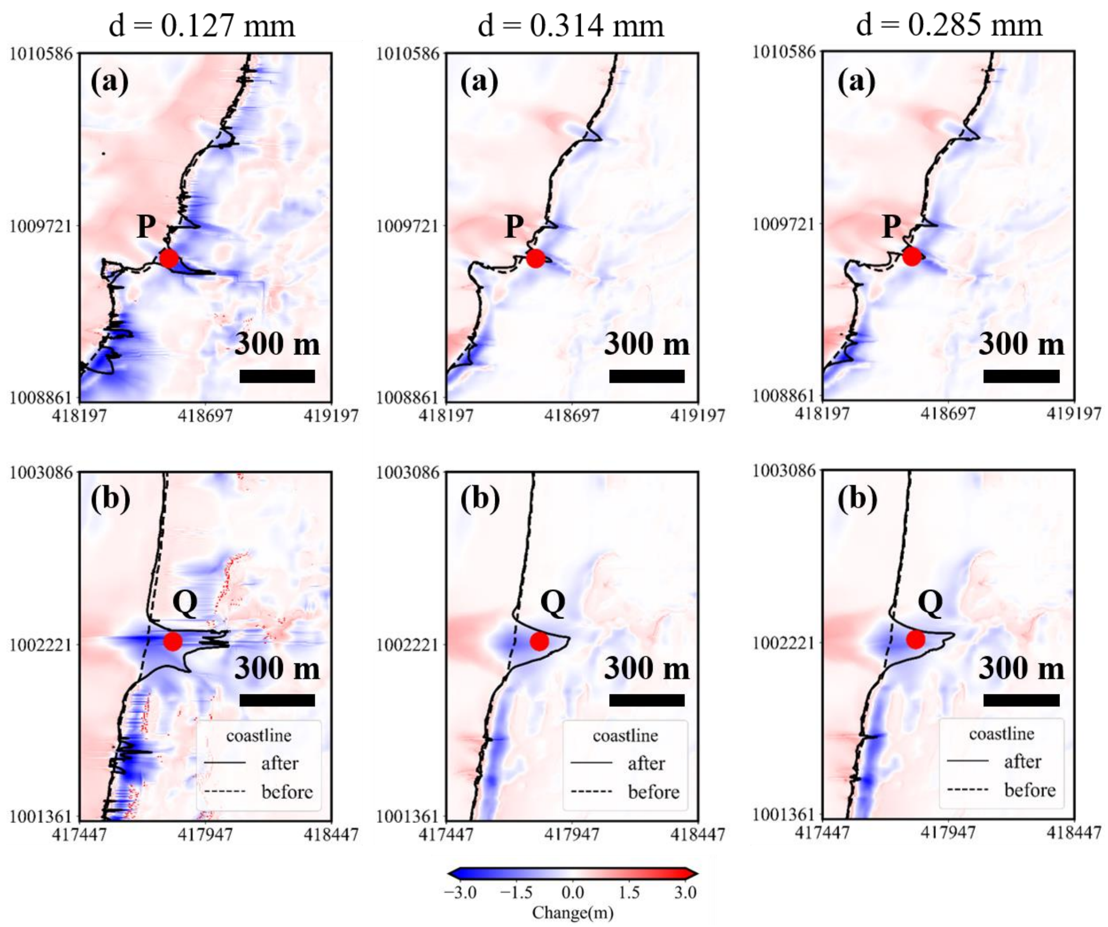

Figure 8 Topographic change and shoreline position caused by the tsunami for each grain size

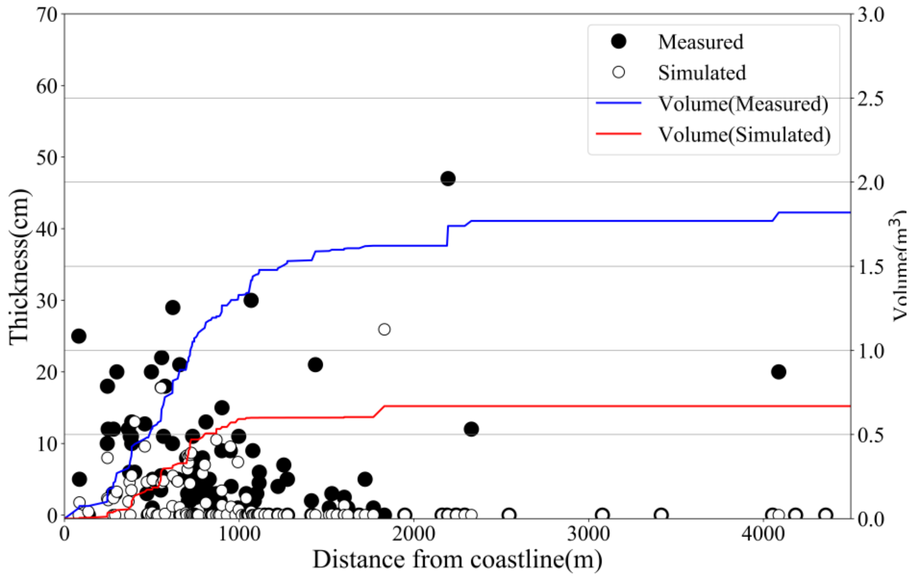

Figure 9 Comparison of field measured and simulated tsunami deposit thickness using a representative grain size of d = 0.314 mm

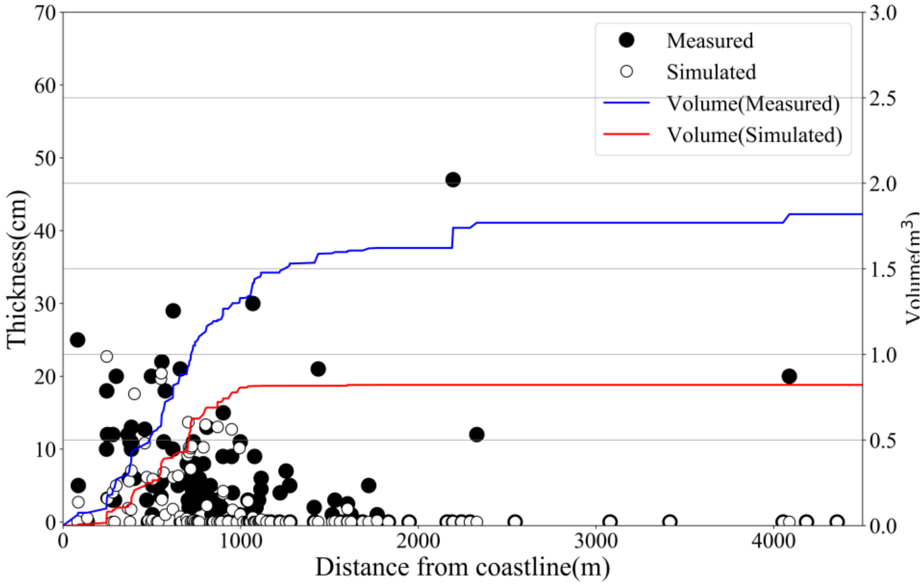

Figure 10 Comparison of field measured and simulated tsunami deposit thickness using a representative grain size of d = 0. 285mm

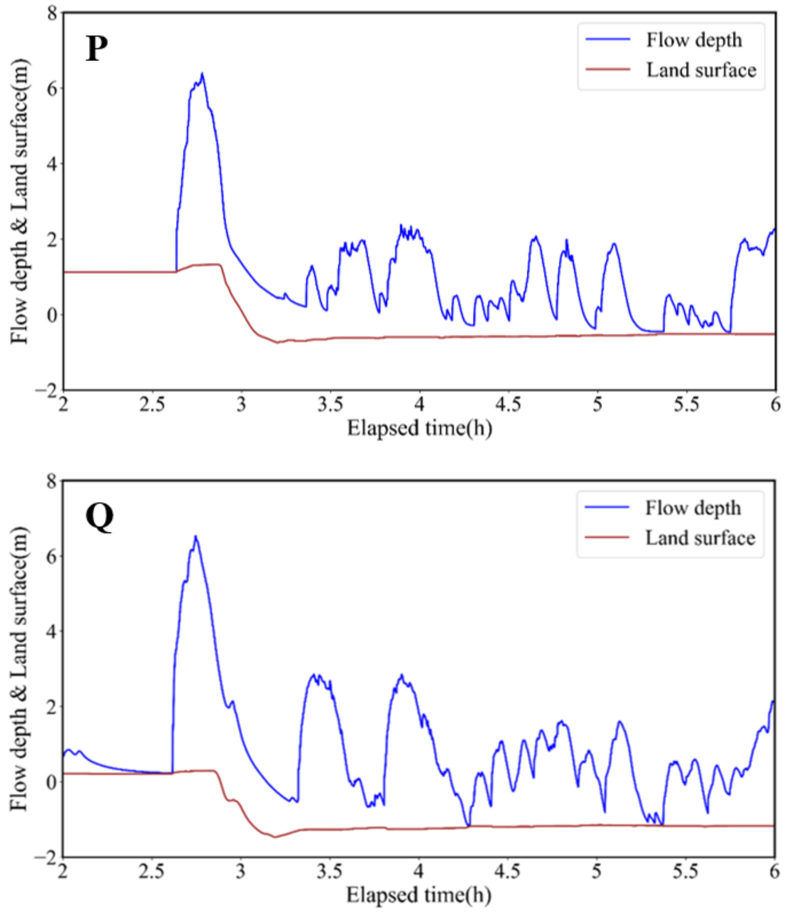

Figure 11 Chronological change of flow depth and land surface at point P and Q in region (a) and (b) (blue line shows the flow depth and red line shows the land surface)

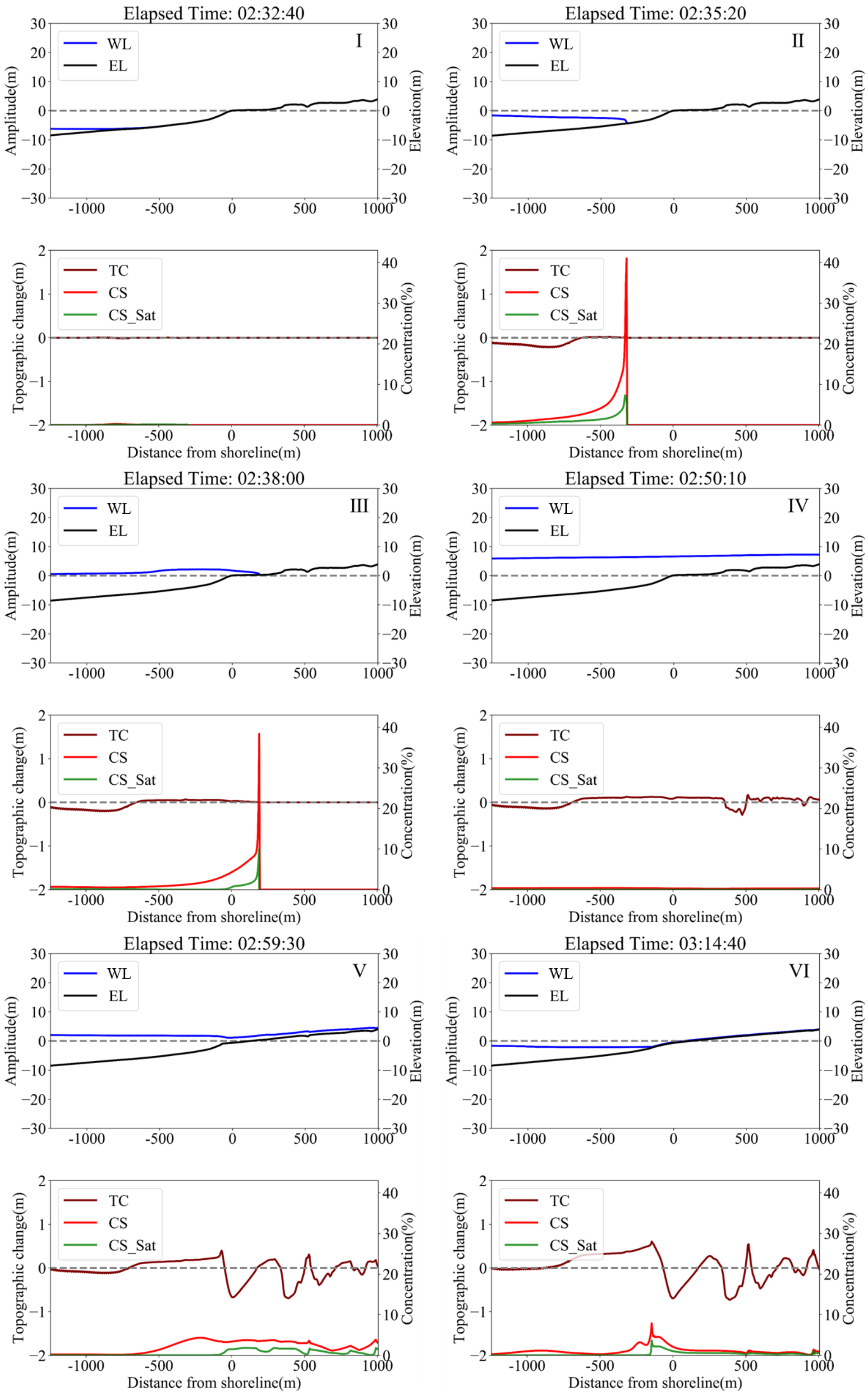

Figure 12 Change in water level (WL), land surface (EL), topographic change (TC), suspended sediment concentration (CS), and saturation suspended sediment concentration (CS_Sat) by section calculation along the survey line in region (b). (I) before the 1st pushing wave, (II) Advance of 1st leading wave in shallow water, (III) Start of 1st leading wave run-up, (IV)Maximum of 1st leading wave , (V) Advance of 2nd backwash, (VI) Maximum of 2nd backwash

3.2. *Sediment transport process*

Although the model reproduces the zones of sediment erosion and deposition well, the sediment transport processes during the tsunami event can be examined by regions (a) and (b) in Figure 5. The modelled time series of the changes of water height and elevation at point P in region (a) and point Q in region (b) are shown in Figure 11. From the modelling results show that the first wave arrived 2 hours 40 minutes after the earthquake, and backwash was generated 10 minutes later (Figure 11). In addition, the ground surface elevation increased by about 30 cm through sediment deposition during the first inflowing wave, and *ca*. 1.5m was eroded during the backwash transporting sediment towards the ocean, so beach loss in both regions is considered to be a result of erosion during the backwash (red line in Figure 11). However, there are two points which shall be highlighted as the points of interest for the initial conditions in the recovery process. First, why was not the beach eroded by the pushing waves? Second, how did the sediment flowing to the seaward in the first wave move?

Based on the waveform (which assumes a flat surface), a cross section calculation was carried out along the transect in Figure 2. Regarding the setting of the transect, one line was set only on the region (b) where the shoreline extends in the normal direction to the direction of the tsunami and the planar effect was considered to be small. Figure 12 shows the changes in ground level, water level, suspended sediment concentration and saturation of suspended sediment concentration on the transect at each unit of time. As shown in Figure 12, prior to the first wave, the ocean receded to below approximately 8 m below mean sea level. As inflow of the first wave began, sediment was eroded from the sea floor at ca. 5-10m below mean sea level. This nearshore erosion increased the suspended sediment concentration as the first wave propagated onshore. At the shoreline, the suspended sediment concentration saturated and sedimentation could begin at the shoreline. In other words, it is estimated that sediment eroded the nearshore (5 m < depth < 10 m) environment during the first inflowing wave, and much of this sediment was transported inland. This could be considered to be the reason that the beach was not eroded by the pushing wave. As inflow terminated, the suspended sediment concentration decreased as sediment settled out of the water column and was deposited inland. Inland, it was found that erosion and deposition occurred according to topographical conditions.

At the initiation of backwash, the suspended sediment concentration is low. As backwash flows towards the ocean, the velocity increases, which increases erosion and causes the suspended sediment concentration to increase. This finding is consistent with the changes recorded in Figure 11. As backwash of the first wave ended, the water still contained a high suspended sediment concentration and this was deposited in the nearshore environment at less than 5 m water depth (Figure 12). While no significant topographic change was found. Thus, this modelling shows that most of the sediment that eroded from the onshore area was deposited in the shallow nearshore zone.

4. Discussion

4.1. *Sediment transport process and beach erosion*

Region (a) and (b) were selected for detailed investigation of the simulation results and discussion.

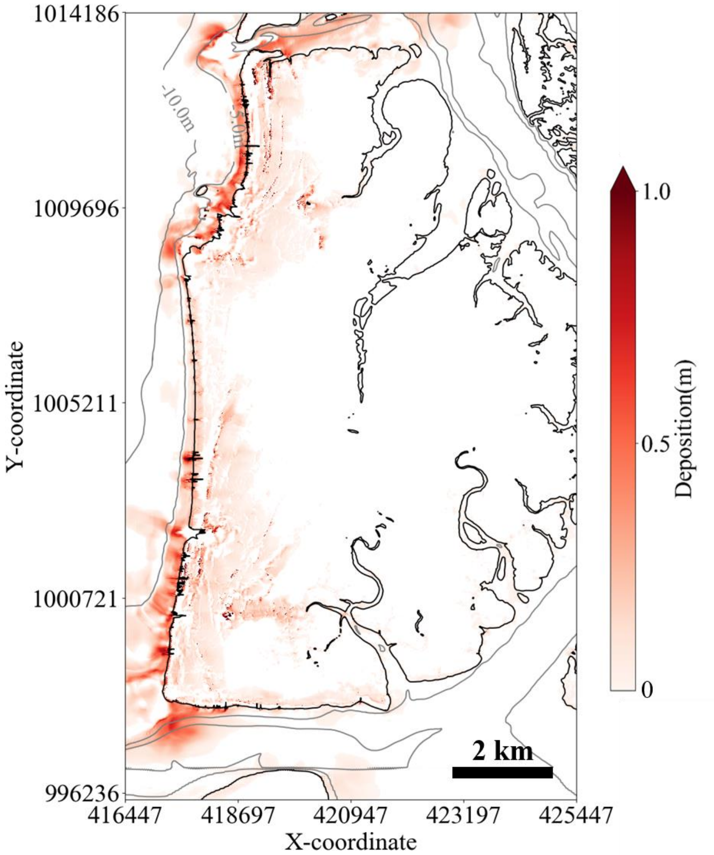

Figure 13 Sediment distribution derived from the simulation (showing depth contours at 5 m intervals in the sea area)

In the sediment transport process on Phra Thong Island, a tsunami wave was large enough to expose the nearshore sediments ran up the exposed nearshore area while retaining sediment from the shallow water. The sediment concentration gradually increases while running up the relatively long distance of the exposed nearshore, and became sediment-saturated as the wave reached the shoreline, making it difficult for new sediment to be eroded further. This can explain why the degree of beach erosion is small during the inflowing wave, and may be a characteristic sediment transport properties of shallow beaches like those on Phra Thong Island. In other words, the numerical simulation results suggest that there is little transportation of sediments from beach by the first inflowing wave and that inland tsunami deposits originated from the nearshore environment. This finding is confirmed by the analysis of microfossils (Sawai et al., 2009) from preserved 2004 IOT tsunami deposits inland that suggested that tsunami deposits on Phra Thong Island originated from the shallow nearshore zone, and Pham et al. (2018) suggested that sediment grain sizes and mineralogy were most similar to those of nearshore sediments. Figure 13 shows the results of the calculated sediment deposition both onshore and offshore Phra Thong Island. From the modelling results, most of the eroded sediment was deposited in shallow nearshore environments in water less than approximately 5 m deep.

The simulations show that the eroded sediments were deposited in the nearshore zone during backwash, which primed the coastal zone for rapid coastal recovery. The removal of sediment from the onshore coastal zone also generated accommodation space that may have contributed to the coastal recovery process. Future studies can build on these findings to determine the extent of sediment transport and deposition, and identify the processes of coastal recovery on Phra Thong Island.

Geomorphologically, the Sendai Plain, which was inundated by the March 11, 2011 Great East Japan tsunami, is similar to the beach ridge plain on Phra Thong Island (Tanaka et al., 2011), but most of the tsunami sediment deposited onshore came from terrestrial sources (Goto et al., 2012; Szczucin´ski et al., 2012; Takashimizu et al., 2012; Sugawara et al., 2014b). However, the Great East Japan tsunami differed from the 2004 IOT as the Japanese event had a much smaller receding wave (Nationwide Ocean Wave information network for Ports and HArbourS, NOWPHAS). As such the Japanese tsunami may not have achieved sediment saturation as the wave approached the shoreline, thereby containing a lower sediment concentration and allowing large volumes of sediment to be entrained from the beach for subsequent formation of inland deposits. The different sources of deposited sediment in the two areas reflects contrasting sediment transport mechanisms on shallow beaches, and may be useful for estimating paleotsunami from coast recovery and geological records.

4.2. *Limits of calculation results*

This study analyzed tsunami sediment transport on Phra Thong Island using numerical calculations and assumed that the island was unvegetated and lacked topography. However, the western half of the island has an undulating surface caused by the beach ridge and swale system, and is extensively vegetated with trees and dense grasses on the ridges and thick grasses within the swales. The eastern half of the island has wide tidal channels and an extensive fringing mangrove system. Both topography and differing vegetation types add complexity to the inundation and backflow sediment transport models not captured here. In future, it is necessary to consider the influence of vegetation on tsunami sediment transport.

Another potential limitation of the model is the selection of a single (median) grain size for the sediments. As shown in previous studies (e.g. Sugawara et al., 2014a), the assumption of transport of single grain sized sediment differs from actual situations because of the distribution of grain sizes mobilised and deposited by tsunami. Therefore, it is important to set representative grain sizes and fully study how grain size affects tsunami sediment transport. Future modelling may consider simulating the suite of grain sizes individually or simulating a population of grain sizes that are identified in the modern environment and in preserved tsunami deposits.

Furthermore, although the calculation was performed considering the entire area a movable bed, the existence of fixed beds, such as rocky areas, should be considered. We consider this a minor component of this research as the rocky headlands that serve as fixed beds are relatively small in area and would contribute little to the overall simulations in our models.

Sugawara et al. (2014b) considers the simulation result of sediment layer thickness using the tsunami sediment transport calculation to be affected by grain size, bottom conditions and topographic data. Their study showed that the layer thickness increases as grain size becomes finer and the layer thickness distribution tendency was unchanged regardless of grain size. Similar results were obtained in this study. Additionally, because bottom surface roughness greatly affects sediment transport near the shoreline, varying bottom surface conditions may influence future modelling results on Phra Thong Island.

5. Conclusion

Because of insufficient knowledge about the topographic recovery process after a tsunami, this study used sediment transport modelling to identify the erosional and depositional processes affecting the coastal zone at Phra Thong Island, Thailand during the 2004 Indian Ocean Tsunami.

First, it was confirmed by comparing simulated results of the shoreline and sediment layer thickness that the location of beach runoff identified on Phra Thong Island was reproducible and consistent with sediment transport results. Based on the sediment transport results we conclude that the processes of sediment erosion and deposition on Phra Thong Island are characterized by the following sequence:

- erosion caused by the inflowing waves occurred at a relatively shallow location in the offshore area and the transported sediment was deposited near the shoreline;
- the inflowing waves caused minimal erosion of the shoreline;
- onshore sediment deposition is due to onshore topographical features trapping sediments prior to backwash; and,
- erosion of the shoreline was largely caused by backwash resulting in onshore sediments deposited in the shallow nearshore zone.

These erosional and depositional processes demonstrate the locations of sediment removal and subsequent deposition during the different phases of the first tsunami wave on Phra Thong Island. The simulations also show that the zones of erosion and deposition across the island and offshore coastal zone are non-uniform. In particular, the zones of erosion and deposition highlighted in the simulations establish the environmental conditions that existed in the transitional phase between catastrophic tsunami and normal coastal processes that facilitated coastal recovery.

6. Acknowledgements

We would like to express our gratitude for the support and data received from Panon Latcharote of the Faculty of Science and Technology of Thammasat University as well as help and support from Prof. Dr. Supot Teachavorasinskun, Dean of Faculty of Engineering, Chulalongkorn University; and the Royal Thai Navy. RM, AS, KY, FI was support by JSPS Grant-in-Aid for Scientific Research (A) No. 17H01631 (FY2017 - FY2021). AS and NL was support by JSPS Bilateral program for joint research with National Research Council of Thailand (NRCT) (FY2017 - FY2018). CG was supported by NUS grant (R-109-000-223-133). NL was supported by Ratchadapisek Sompoch Endowment Fund (2019), Chulalongkorn University (762003-CC). This work is a contribution to IGCP Project 639, 'Sea-level Change from Minutes to Millennia'.

References

1) Abe, T., Goto, K., and Sugawara, D.: Relationship between the maximum extent of tsunami sand and the inundation limit of the 2011 Tohoku–oki tsunami on the Sendai Plain, Japan, Sedimentary Geology, 282, 142–150, 2012.
2) Aida, I.: Reliability of a tsunami source model derived from fault parameters, J. Phys. Earth, 26, 57–73, 1978.
3) Apotsos, A., Buckley, M., Gelfenbaum, G., Jaffe, B., and Vatvani, D.: Nearshore tsunami inundation model validation: toward sediment transport applications. Pure and Applied Geophysics, 168, 2097-2119, 2011a.
4) Apotsos, A., Gelfenbaum, G., and Jaffe, B.: Process-based modeling of tsunami inundation and sediment transport, Journal of Geophysical Research, 116, F01006, 2011b.
5) Apotsos, A., Gelfenbaum, G., Jaffe, B., Watt, S., Peck, B., Buckley, M., and Stevens, A.: Tsunami inundation and sediment transport in a sediment-limited embayment on American Samoa: Earth-Science Reviews, 107, 1-11, 2011c.
6) Brill, D., Klasen, N., Jankaew, K., Brückner, H., Kelletat, D., Scheffers, A., and Scheffers, S.: Local inundation distances and regional tsunami recurrence in the Indian Ocean inferred from liminescence dating of sandy deposits in Thailand, Natural Hazards and Earth System Sciences, 12, 2177–2192, 2012.
7) Brill, D., Klasen, Brückner, H., Jankaew, K., Scheffers, A., Kelletat, D., and Scheffers, S.: OSL dating of tsunami deposits from Phra Thong Island, Thailand, Quaternary Geochronology, 10, 224–229, 2012.
8) Brill, D., Jankaew, K., Bruckner, H.: Holocene evolution of Phra Thong's beach-ridge plain (Thailand) — Chronology, processes and driving factors, Geomorphology, 245, 117–134, 2015.
9) ChaguéGoff, C., Andrew, A., Szczuciński, W., Goff, J., and Nishimuira, Y.: Geochemical signatures up to the maximam inundation of the 2011 Tohoku–oki tsunami — Implications for the 869 AD Jogan and other palaeotsunamis, Sedimentary Geology, 282, 65–77, 2012.
10) Choowong, M., Phantuwongraj, S., Charoentitirat, T., Chutakositkanon, V., Yumuang S., and Charusiri, P.: Beach recovery after 2004 Indian Ocean tsunami from Phang–nga, Thailand, Geomorphology, 104, 134–142, 2009.
11) Fagherazzi, S. & Du, X.: Tsunamigenic incisions produced by the December 2004 earthquake along the coasts of Thailand, Indonesia and Sri Lanka, Geomorphology, 99, 120–129, 2008.
12) Feldens, P., Schwarzer, K., Szczuciński, W., Stattegger, K., Sakuna, D. and Somgpongchaiykul, P. Impact of 2004 tsunami on seafloor morphology and offshore sediments, Pakarang Cape, Thailand, Polish Journal of Environmental Science Vol. 18, No. 1 (2009), 63-68
13) Fujino S., Naruse H., Matsumoto, D., Jarupongsakul T., Sphawajruksakul A., and Sakakura, N.: Stratigraphic evidence for pre–2004 tsunamis in southwestern Thailand, Marine Geology, 262, 25–28, 2009.
14) Fujino, S., Naruse, H., Matsumoto, D., Sakakura, N., Suphawajruksakul, A., and Jarupongsakul,

T.: Detailed measurements of thickness and grain size of a widespread onshore tsunami deposit in Phang–nga Province, southwestern Thailand, Island Arc, 19, 389–398, 2010.

15) Gelfenbaum G., Vatvani D., Jaffe B., and Dekker F.: Tsunami inundation and sediment transport in vicinity of coastal mangrove forest, Coastal Sediments, 07, 1117-1128, 2007.

16) Goto, K., Takahashi, J., Oie, T., and Imamura, F.: Remarkable bathymetric change in the nearshore zone by the 2004 Indian Ocean tsunami: Kirinda Harbor, Sri Lanka, Geomorphology, 127, No.1-2, 107–116, 2011a.

17) Goto, K., ChaguéGoff, C., Fujino, S., Goff, J., Jaffe B., Nishimura, Y., Richmond, B., Sugawara, D., Szczuciński, W., Tappin, R. D., Witter, C. R., and Yuliant, E., New insights of tsunami hazard from the 2011 Tohoku–oki event, Marine Geology, 290, 46–50, 2011b.

18) Goto, K., Chague´Goff, C., Goff, J., and Jaffe, B.: The future of tsunami research following the 2011 Tohoku–oki event, Sedimen- tary Geology, 282, 1–13, 2012.

19) Gouramanis, C., Switzer, A. D., Polivka, P. M., Bristow, C. S., Jankaew, K., Dat, P. T., Pile, J., Rubin, C. M., Yingsin, L., Ildefonso, S. R., and Jol, H. M.: Ground penetrating radar examination of thin tsunami beds - A case study from Phra Thong Island, Thailand,Sediment. Geol., 329, 149–165, 2015.

20) Gouramanis, C., Switzer, A. D., Jankaew, K., Bristow, C. S., Pham, D. T., and Ildefonso, S. R.: High-frequency coastal overwash deposits from PHRA thong Island, Thailand, Sci. Rep., Vol.7, No. September 2016, 1–9, 2017.

21) Gusman, A. R., Tanioka, Y., and Takahashi, T.: Numerical experiment and a case study of sediment transport simulation of the 2004 Indian Ocean tsunami in Lhok Nga, Banda Aceh, Indonesia., Earth, planets and space, 64, 817-827, 2012.

22) Haraguchi, T., Takahashi, T., Hisamatsu, R., Morishita, Y., and Sasaki, I.: A Field Survey of Geomorphic Change on Kessennuma Bay caused by the 2010 Chilean Tsunami and the 2011 Tohoku Tsunami, Journal of JSCE, B2 (Coastal Engineering), 68, 231–235, 2012.

23) Hawkes, A.D., Bird, M., Cowie, S., Grundy-Warr, C., Horton, B.P., Hwai, A.T.S., Law, L., Macgregor, C., Nott, J., Ong, J.E., Rigg, J., Robinson, R., Tan-Mullins, M., Sa, T.T., Yasin, Z., Aik, L.W.: Sediments deposited by the 2004 Indian Ocean Tsunami along the Malaysia–Thailand Peninsula, Marine Geology, 242, 169–190, 2007.

24) Hirao, R., Tanaka, H., Umeda, M., Adityawan, M. B., Mano, A., and Udo, K.: Breaching of Sandy Coast and Spit Due To The 2011 Tsunami and Their Recovery, Journal of JSCE, B2(Coastal Engineering), 68, 581–585, 2012.

25) Imai, K., Sugawara, D., Takahashi, T., Iwama, S., and Tanaka, H.: Numerical study for sediment transport due to tsunami around the Kitakami River mouth, Journal of JSCE, B2(Coastal Engineering), 71, 247–252, 2015.

26) Iwagaki, Y.: Hydrodynamical study on critical tractive force, Trans. JSCE, 41(41), 1–21, 1956.

27) Jankaew, K., Atwater, B. F., Sawai, Y., Choowong, M., Charoentitirat, T., Martin, M. E., and Prendergast, A.: Medieval forewarning of the 2004 Indian Ocean tsunami in Thailand, Nature,

455(7217), 1228–1231, 2008.

28) Koiwa, N., Takahashi, M., Sugisawa, S., Ito, A., Aki Matsumoto, H., Tanavud, C., and Goto, K.: Barrier spit recovery following the 2004 Indian Ocean tsunami at Pakarang Cape, southwest Thailand, Geomorphology, 306, 314–324, 2018.

29) Li, L., Qiu, Q., and Huang, Z.: Numerical modeling of the morphological change in Lhok Nga, west Banda Aceh, during the 2004 Indian Ocean tsunami: understanding tsunami deposits using a forward modeling method, Natural Hazards, 64, 1549-1574, 2012.

30) Li, L., Huang, Z., and Qiu, Q.: Numerical simulation of erosion and deposition at the Thailand Khao Lak coast during the 2004 Indian Ocean tsunami, Natural Hazards, 74, 2251-2277, 2014.

31) Liew, S.C., Gupta, A., Wong, P.P., Kwoh, L.K.: Recovery from a large tsunami mapped over time: The Aceh coast, Sumatra, Geomorphology, 114, 520–529, 2010.

32) Morishita, Y., and Takahashi, T.: Accuracy improvement of movable bed model for tsunamis by applying for Kesennuma bay when the 2011 Tohoku tsunami arrived, Journal of JSCE, B2(Coastal Engineering), 70, 491–495, 2014.

33) Saegusa, S., Tanaka, H., and Mitobe, Y.: Recovery processes of bathymetry of Sendai Bay after the 2011 tsunami, Journal of JSCE, B2(Coastal Engineering), 73, 817–822, 2017.

34) Okada, Y.: Surface deformation due to shear and tensile faults in a half-space, Bulletin of the Seismological Society of America, 75(4), 1135–1154, 1985.

35) Pari, Y., Ramana Murthy, M. V., Jaya Kumar, S., Subramanian, B. R., and Ramachandran, S.: Morphological changes at Vellar estuary, India — Impact of the December 2004 tsunami, Journal of Environmental Management, 89, 45–57, 2008.

36) Paris, R., Lavigne, F., Wassmer, P., Sartohadi, J.: Coastal sedimentation associated with the December 26, 2004 tsunami in Lhok Nga, west Banda Aceh (Sumatra, Indonesia), Marine Geology, 238, 93–106, 2007.

37) Pham, T. D., Gouramanis, C., Switzer, M. A., Rubin, M. C., Jones, G. B., Jankaew, K., and Carr, F. P.: Elemental and mineralogical analysis of marine and coastal sediments from Phra Thong Island, Thailand: Insights into the provenance of coastal hazard deposits, Marine Geology, 385, 274–292, 2018.

38) Prendergast, L. A., Cupper L. M., Jankaew, K., and Sawai, Y.: Indian Ocean tsunami recurrence from optical dating of tsunami sand sheets in Thailand, Marine Geology, 295–298, No.15, 20–27, 2012.

39) Sawai, Y., Jankaew K., Martin, E. M., Prendergast, A., Choowong, M., and Charoentitirat, T.: Diatom assembles in tsunami deposits associated with th 2004 Indian Ocean tsunami at Phra Thong Island, Thailand, Marine Micropaleontology, 73, 70–79, 2009.

40) Sugawara, D., Goto, K., and Jaffe, B. E.: Numerical models of tsunami sediment transport –Current understanding and future directions, Marine Geology, 352, 295–320, 2014a.

41) Sugawara, D., Takahashi, T., and Imamura, F.: Sediment transport due to the 2011 Tohoku-oki tsunami at Sendai: Results from numerical modeling, Mar. Geol., 358, 18–37, 2014b.

42) Suppasri, A., Koshimura, S., and Imamura, F.: Developing tsunami fragility curves based on the satellite remote sensing and the numerical modeling of the 2004 Indian Ocean tsunami in Thailand, Nat. Hazards Earth Syst. Sci., 11(1), 173–189, 2011.
43) Suppasri, A., Latcharote, P., Bricker, J. D., Leelawat, N., Hayashi, A., Yamashita, K., Makinoshima, F., Roeber, V. and Imamura, F. (2016) Improvement of tsunami countermeasures based on lessons from the 2011 great east japan earthquake and tsunami -Situation after five years-, Coastal Engineering Journal, 58 (4), 1640011.
44) Switzer, A.D., Srinivasalu, S., Thangadurai, N., Ram Mohan, V.: Bedding structures in Indian tsunami deposits that provide clues to the dynamics of tsunami inundation, Geological Society, London, Special Publications, 361, 61-77, 2012.
45) Szczuciński, W., Kokociński, M., Rzeszewski, M., Chahué–Goff, C., Cachão, M., Goto, K., and Sugawara, D.: Sediment sources and sedimentation processes of 2011 Tohoku–oki tsunami deposits on the Sendai Plain, Japan — Insights from diatoms, nannoliths and grain size distribution, Sedimentary Geology, 282, 40–56, 2012.
46) Takahashi, T., Shuto, N., Imamura, F., and Asai, D.: Modeling sediment transport due to tsunamis with exchange rate between bed load layer and suspended load layer, Proceedings Of International Conference of Coastal Engineering, 1508–1519, 2000.
47) Takahashi, T., Kurokawa, T., Fujita, M., and Shimada, H.: Hydraulic experiment on sediment transport due to tsunamis with various sand grain size, Journal of JSCE, B2(Coastal Engineering), 67, 231–235, 2011.
48) Takashimizu, Y., Urabe, A., Suzuki, K., and Sato, Y.: Deposition by the 2011 Tohoku–oki tsunami on coastal lowland controlled by beach ridges near Sendai, Japan, Sedimentary Geology, 282, 124–141, 2012.
49) Tanaka, H., Mano, A., and Udo, K.: Beach Morphology Change Induced by The 2011 Great East Japan Earthquake Tsunami, Journal of JSCE, B2(Coastal Engineering), 67(2), 571–575, 2011.
50) Udo, K., Tanaka, H., Mano, A., and Takeda, Y.: Beach Morphology Change of Southern Sendai Coast due to 2011 Tohoku Earthquake Tsunami, Journal of JSCE, B2(Coastal Engineering), 69, 391–395, 2013.
51) Udo, K., and Takeda, Y.: Comparison between characteristics of shoreline changes due to the 2004 Indian Ocean tsunami and the 2011 Great East Japan tsunami, Journal of JSCE, B3(Coastal Engineering), 72, 175–180, 2016.
52) Yamashita, K., Sugawara, D., Takahashi, T., Imamura, F., Saito, Y., Imato, Y., Kai, T., Uehara, H., Kato, T., Nakata, K., Saka, R., and Nishikawa, A.: Numerical simulation of large-scale sediment transport due to the 2011 tohoku earthquake tunami in Rikuzentakata city, Journal of JSCE, B2(Coastal Engineering), 71, 499–504, 2015.
53) Yamashita, K., Sugawara, D., Takahashi, T., Imamura, F., Saito, Y., Imato, Y., and Saka, R.: Numerical simulations of large-scale sediment transport caused by the 2011 Tohoku Earthquake Tsunami in Hirota Bay, Southern Sanriku Coast. Coastal Engineering Journal, 58(04), 2016.

54) Yamashita, K., Shigihara , Y., Sugawara, D., Arikawa, T., Takahashi, T., and Imamura, F.: Effect of sediment tansport on tsunami hazard and building damage –an integrated simulation of tsunami inundation, sediment transport and drifting vessels in Kesennuma city, Miyagi prefecture during the great east Japan –, Journal of JSCE, B2(Coastal Engineering), 73, 355–360, 2017.

55) Yamashita, K., Sugawara, D., Arikawa, Y.., Takahashi, T., and Imamura, F.: Improvement of tsunami-induced sediment transport model by considering saturated concentration in suspension with strong unsteady flows, Journal of JSCE, B2(Coastal Engineering), 69, 325–330, 2018.

56) Yunus Ali, P., and Narayama, A. C.: Short–Term Morphological and Shoreline Changes at Trinkat Island, Andaman and Nicobar, India, After the 2004 Tsunami, Marine Geodesy, 38, 26–39, 2015.